24th COBEM - 2017

24th ABCM International Congress of Mechanical Engineering
December 3-8, 2017, Curitiba, PR, Brazil

COBEM-2017- 0098
DRILLING OF HIGH STRENGTH GREY IRON, GRADE 300, WITH REFINED GRAPHITE AND MO ADDITION

Aline Elias da Silva
Alcione dos Reis
Federal University of Uberlândia - Uberlândia, MG, Brazil
alinengelias@gmail.com and alcionedosreis@yahoo.com.br

Álisson Rocha Machado
Pontifical Catholic University of Paraná - Curitiba, PR, Brazil
Federal University of Uberlândia - Uberlândia, MG, Brazil
alisson.rocha@pucpr.br

Wilson Luiz Guesser
Santa Catarina State University - Joinville, SC, Brazil
TUPY. S.A. - Joinville, SC, Brazil
wguesser@tupy.com.br

Abstract. *The present study aims to evaluate the machinability of FC-300 gray cast iron – high resistance class with refined graphite and addition of molybdenum, for use in engine cylinder heads, compared with a material already used for this purpose, the FC-250 gray cast iron. The drilling process was been chosen for the tests because this process is widely used in the manufacture of engine heads. A drill with steel body and indexable cemented carbide tips were used in the experiments. The tool life, with identification of the tool wear mechanisms, the thrust force and torque and quality of machined holes (roughness, roundness and cylindricity) were the output variables considered. To assist in the discussion of the results the materials were characterized according to the interlamelar spacing and microhardness of the pearlite matrix, to the number of eutectic cells and to the distribution of inclusions of manganese sulfide. In general, the results show that FC-300 iron showed the poorer machinability than the FC-250 and that there are good relationships between the microstructural characteristics and their machinability.*

Keywords: *machinability, cast iron, microstructural characteristics, drilling, tool wear*.

1. INTRODUCTION

The gray cast iron, a material with long tradition of the automotive sector, still represents one of the cast materials of high global production. Features like good castability, excellent machinability, low cost, vibration damping capacity and good thermal conductivity justify the use of this material in various engineering components, among which stand out the cylinder blocks and cylinder heads for diesel engines.

Therefore, the possibility of improving the mechanical properties of this material is of great interest to the automotive industry. More resistant materials enable the manufacture of engine components with lighter weight and better performance which, in turn, helps to reduce emissions.

Therefore, in order to address these issues, the gray cast iron needs to receive the addition of alloying elements and also special inoculation treatments (the latter to promote the refinement of the microstructure), both aiming at improving the mechanical properties of these materials. However, the use of more resistant materials may result in machining problems because of the lower productivity and higher costs with cutting tools. According to Marquard *et al.* (1998), the choice of a material for use in the automotive industry must be grounded on the following characteristics: weight, strength, material cost, environmental considerations and cost of machining.

In general, the mechanical strength of cast iron and, consequently, their grades are conditioned to its final structure obtained. Thus, such a property depends on the shape and quantity of graphite and the amount of ferrite and / or pearlite in the metallic matrix. The resistance is increased with increased pearlite content and also with decreasing interlamellar spacing of the pearlite (TUPY, 2014; GUESSER, 2009).

Gray cast iron is presently a material traditionally used in many industrial applications because of their excellent performance in machining processes, damping capability wear resistance, fatigue strength, among others. Thus, the possibility of improving the mechanical properties of this material is of great industrial interest. Many designers may prefer compact graphite iron or nodular cast iron, when high tensile strength is required, even though these materials are more expensive than gray iron (AZTERLAN, 2013).

The usual mechanism for raising the tensile strength and hardness of gray cast iron is the addition of alloying elements such as chromium (Cr), molybdenum (Mo), tin (Sn) and copper (Cu). Additional amounts of copper and tin promote the refinement of the pearlite or reduction in the interlamellar spacing, resulting in increased strength. Cr and Mo act in the formation of carbides and, as Sn and Cu, Mo can be used also as a refiner of the pearlite (Röhrig, 1981).

Reduction of the carbon content from 3.2 to 3.0% results in smaller graphite lamellae, thus reducing the risk of crack initialization and propagation. Moreover, it is obtained from it, an increase of 10 to 20% in the mechanical properties (DAWSON, 2009). However, these changes significantly affect some of the advantages of gray iron, for example, its machinability.

In the casting process, as well as the chemical composition, the cooling rate in solid state, can also significantly influence the mechanical properties of the materials. An increase in the cooling rate will refine both the graphite and the matrix structure (increasing the amount of pearlite), resulting in an increase in hardness and strength (RÖHRIG, 1981; ASM, 1990a).

During chip formation of gray cast iron, the material compressed by the tool presents sharp lamellae. Thus, there is a stress concentration at the ends of the graphite particles and because they are interconnected, crack propagation plans are created ahead of the cutting edge. With the movement of the tool, the material is completely removed with lower shear stress (MARWANGA, 1999, MARWANGA, 2000).

Regarding to ferrous materials, the hardness is considered to be a reasonable machinability index. However, as to gray cast iron microstructure is the key indicator. A reduction in the ferrite content or decreasing the interlamellar spacing of the pearlite lowers the machinability of this material (ASM, 1990b; ASM, 1989).

In Tab. 1 it is observed that the tool wear rate increases with increasing pearlite proportions in the matrix and with decreasing in interlamellar spacing (refined pearlite). Moreover, the excess of iron carbide in the pearlite matrix promotes additional increase in the wear rate.

Table 1. Effect of the microstructure of the gray irons in tool life (ASM, 1989).

Microstructure of the matrix	Brinell Hardness	Machinability Index
ferrite	121-179	250
50% of ferrite and 50% of pearlite	131-189	300
Coarse pearlite	143-207	300
Medium pearlite	163-229	350
Fine pearlite	197-255	400
Fine pearlite with 5% of excess of Fe_3C	207-269	450

According to Guesser (2009), the machinability of gray cast irons decreases as we move to higher strength grades, because of the increased abrasiveness with increasing amount of pearlite in the matrix and also because of the reduction of lubricating action and consequent reduction in the facility of breaking the chips with reduced amount of graphite.

Furthermore, there is a decrease in the machinability index as the cementite fraction in the pearlite increases. Bates (1986) showed the influence of the percentage of Fe_3C in the tool life in drilling of gray cast iron with HSS drills (Fig. 1). It is observed that the increasing amount of cementite in the pearlite results in a reduction in the number of holes produced.

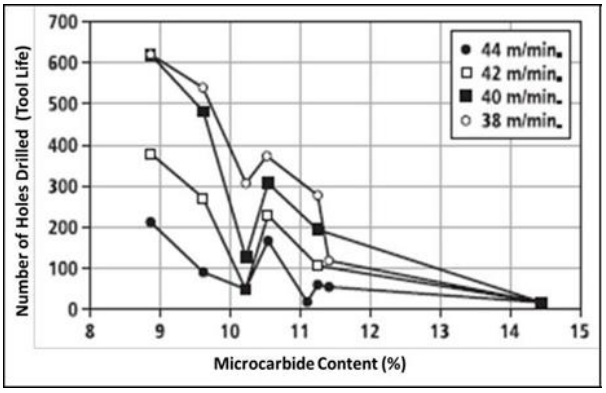

Figure 1. Effect of carbide content in pearlite in gray iron on tool life (BATES, 1986)

The present study aims to evaluate the machinability of high strength FC300 gray cast iron with the addition of molybdenum and graphite refining for use in engine heads. For comparison purposes, the FC250 gray cast iron was also investigated.

2. MATERIALS AND METHODS

2.1 Characterization of the Materials

The materials tested were the FC-250 gray cast iron (FC250) and gray FC-300 gray cast iron with high strength by the addition of Mo in its microstructure and graphite refining ($FC300_{RG}$).

The micrographs of these materials, obtained in a Scanning Electron Microscope (SEM - Hitashi TM 3000) as well as micrographs showing 100% pearlitic matrix on both, obtained by optical microscopy (Olympus microscope) are presented in Fig. 2.

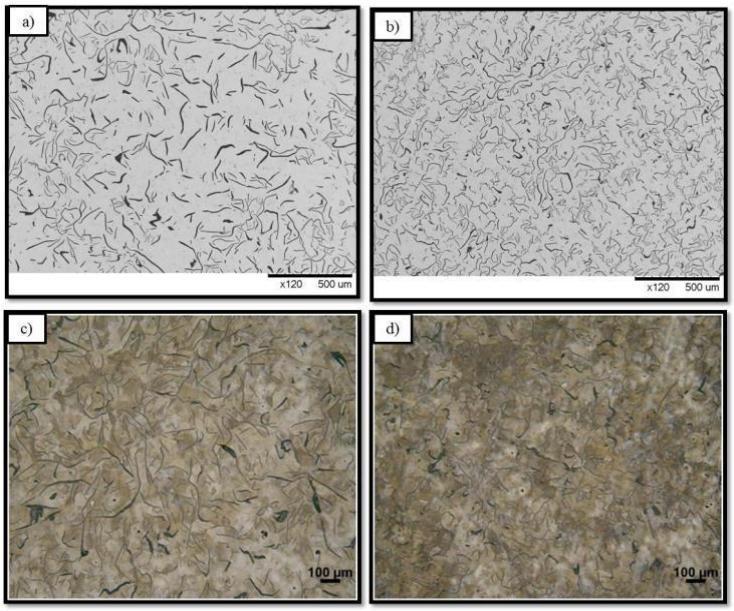

Figure 2. Microstructure of: a) FC250 and b) $FC300_{RG}$ (SEM); c) FC250 and $FC300_{RG}$ (Optical microscopy)

The morphology of the graphite on both gray irons are of fine and uniform lamellae with random orientation, typical of type I and pattern A (ASTM A247, 2010). Fig. 2 also shows the fine aspect of the graphite in the $FC300_{RG}$ gray cast iron.

Metallographic analysis allowed eutectic cell counting for both materials, resulting in 170 eutectic cells/cm2 for the FC250 and 350 eutectic cells/cm2 for the $FC300_{RG}$. This information about the metallography of gray cast irons is very important for analysis the machining results of these materials, since the quantity of eutectic cells directly reflected on the volume and size of graphites. A greater number of cells tend to have a finer structure with smaller size of graphite,

which reduces the crack propagation condition, thus hampering machining. Therefore, based on this information, it is expected a poorer machinability of $FC300_{RG}$.

Table 2 shows the Brinell hardness of the materials, the Vickers microhardness of the pearlite and the mechanical strength of both materials.

Table 2. Hardness and strength of the gray cast irons.

Properties	FC250	$FC300_{(RG)}$
Hardness [HB]	187	217
Microhardness of the pearlite [HV]	280	309
UTS [MPa]	259	283

To assess the amount and area of manganese sulfide (MnS) particles distributed in the material matrix, an Olympus optical microscope (model BX51) and the Stream Essentials 1.9.4 software (Olympus) were used on areas of 0.05 mm^2. Ten images with magnification of 500x were used to determine the amount of MnS inclusions/mm^2 in each grade of gray irons tested. For the evaluation of the area, 150 particles of MnS were randomly selected in images with magnification levels also of 500x. Figure 3a shows an example of how the area of the particles was measured.

The determination of the interlamellar spacing of the pearlite was performed using SEM images. Twenty-five images with 20000x magnification were taken in different regions randomly selected for measuring the intersections of cementite lamellae, using the following criteria (VOORT and ROOSZ, 1984):

1. Selection of pearlite colonies with the lowest field spacing;
2. With the help of Image J (Image Processing and Analysis in Java 1.5) software a line was drawn (Fig. 3b) perpendicular to the cementite lamellae, whose known length was 3.7 μm;
3. The length of this line was divided by the number of cementite lamellae that cut this line. The result of this division was considered the interlamellar spacing of the pearlite

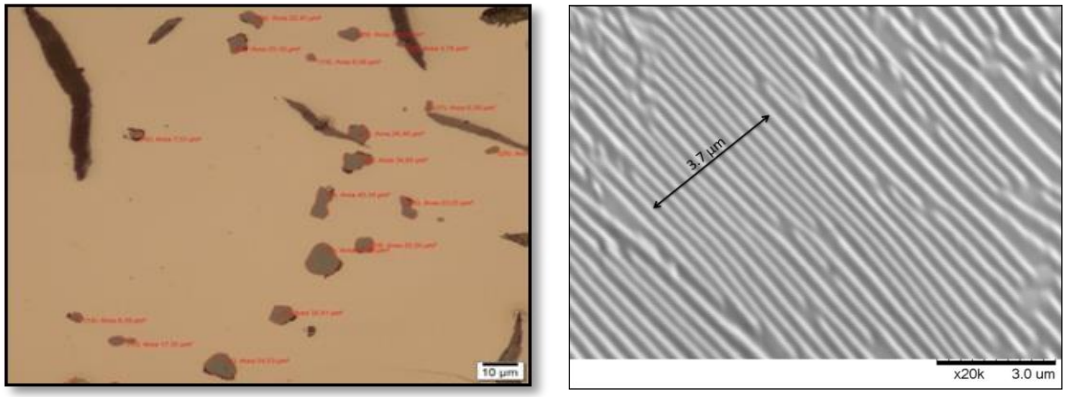

Figure 3. a) Identification of the MnS inclusions; b) Determination of the interlamellar spacing of the pearlite

2.2 Workpiece samples, cutting tools and drilling tests

The work materials were provided by Tupy S.A in the form of rectangular bars whose dimensions were approximately 400 mm long, 240 mm wide and 40 mm thick. Five hundred and eighty nine (589) holes of 10 mm of diameter, with 2 mm of distance between them were machined in each bar. These workpiece samples were pre-machined (flattened) on both sides to maintain a standard thickness of 36 mm. The cutting tools used in this research were SUMOCHAM drills, with steel body (10 mm of diameter) and cemented carbide indexable drill tips (K20 class - K40) with TiAlN coatings, manufactured by ISCAR Ltda.

The tool life tests followed a 23 factorial design, consisting of two quantitative variables, cutting speed (Vc) and feed rate (f), and one qualitative variable, the work material. All tests were repeated twice, totaling three tests in each condition (test and two replicas). Table 3 shows the input variables and their two levels.

Blind holes were machined in dry condition (without cutting fluid), with a fixed length (Lf) of 16 mm, in a CNC vertical machining center DISCOVERY 760 manufactured by Romi/Bridgeport. Dry drilling process was used to accelerate the tool life tests and the fluid was not a variable under study. For the tool life tests was used an end of tool life criterion based on maximum flank wear (VB_{Bmax}) equal to 0.40 mm or a maximum of 500 holes in cases where the tool wear rates were too slow.

Table 3. Input variables at two levels.

Input variable	Level (- 1)	Level (+ 1)
V_c (m/min)	70	140
f (mm/rev)	0.15	0.25
Work material	FC250	$FC300_{RG}$

After the tool life tests the worn areas of the tools were analyzed within the scanning electron microscopy – SEM. However, because of the great amount of adherent work material on the tool surfaces it was necessary to remove them by chemical etching (Nital 4%).

Furthermore, specific tests were performed in order to monitor the thrust force and torque, as well as for measuring the surface roughness, roundness, and cylindricity. In these tests a new tool was always used when the maximum flank wear (VB_{Bmax}) reached 0.1 mm, to avoid the influence of tool wear on the results. One variable at a time method was used in these tests. Firstly the cutting speed was varied and the feed rate was kept constant and vice-versa. A test and two replicas were performed for statistic purposes. The tests were performed dry and the cutting conditions are given in Tab. 4.

Table 4. Cutting conditions used in the specific tests.

Tests	Vc (m/min)	f (mm/rev)	Lf (mm)
Varying the cutting speed	110 - 140	0.27	16
Varying the feed rate	135	0.20 – 0.32	

To measure the thrust force and torque a 9124B Kislter rotating dynamometer, and a 5223B signal amplifier, also manufactured by Kistler Instruments, a data acquisition card (USB 6000) manufactured by National Instrument and the Signal Express® 14.0 software were used. The data acquisition rate was 1000 Hz and the acquisition time being dependent on the cutting parameters.

For measuring the surface roughness parameter *Ra* a Taylor Robson Surftest 201 roughness meter was used. This instrument has a needle probe with diamond tip radius of 5 µm and a resolution of 0.1 µm. A filter (cut-off) of 0.8 mm was used following recommendation of ABNT/ISO 4288 standard (ABNT, 2008). Finally, measurements related to roundness and cylindricity deviations were made in a Coordinate Measuring Machine model BR M443 manufactured by Mitutoyo with 0.001 mm resolution. All measurements were performed at room temperature of 20 ± 1°C, monitored by a digital thermohygrometer, with resolution of 0.1°C and measuring range of -20 to 60°C.

3. RESULTS AND DISCUSSION

3.1 Distribution of MnS particles and interlamellar spacing of the pearlite of the gray cast irons

The results of the average amount of MnS / mm² and the area of manganese sulfide inclusions on the gray cast iron are given in Fig. 4. In Fig. 4a it is observed that there are minor differences in the average amount of MnS inclusions per square millimeter for the two materials. The $FC300_{RG}$ has, on average, 412 MnS particles / mm², while the FC250 has approximately 394 MnS particles / mm². It is also observed (Fig. 4b) that most of MnS particles present in the gray cast irons have areas between 6 and 30 µm².

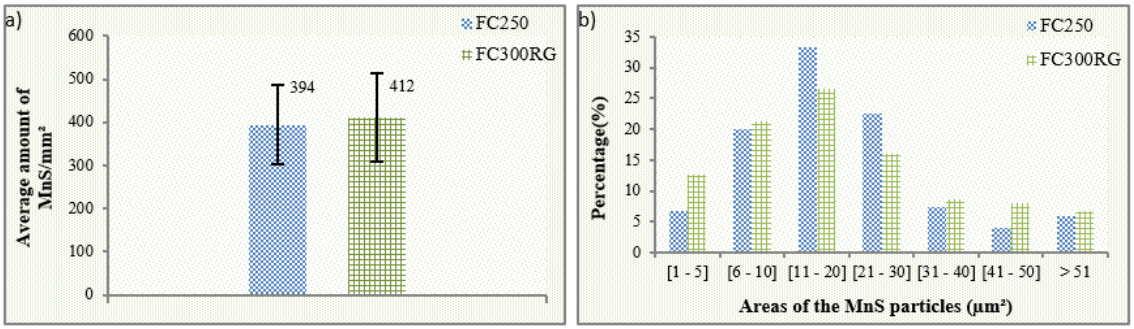

Figure 4. a) Average amount of MnS particles per mm²; b) Areas of the MnS particles

The results of the interlamellar spacing of the pearlite of tested materials are shown in Fig. 5. Note that, in terms of average values, the FC300RG has the lowest interlayer spacing, an average 0.29 µm. Thus, this factor may have influenced the hardness of this material, which was higher than the FC250 (Tab. 2). This may indicate that for the gray cast iron with refined graphite there will be an increase in tensile strength and abrasiveness, making it more difficult to machine.

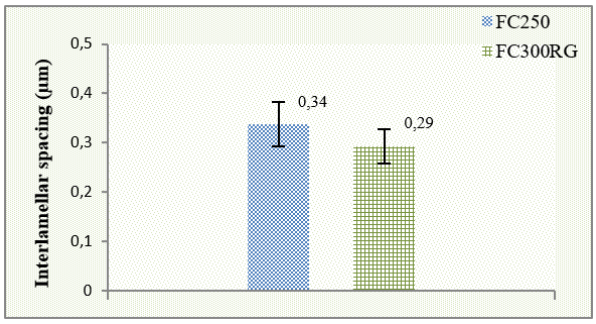

Figure 5. Interlamellar spacing of the pearlite

3.2 Tool life and tool wear mechanism analysis

Figure 6 shows the results of tool life in the machining of the two materials in the four cutting conditions tested (Tab. 3), which is evident the high effect of the cutting speed in the machining of the two gray cast irons investigated. Taking as an example, the performance of the tool used to machine the FC250 when the cutting speed was change from 70 m/min to 140 m/min, for the feed rate of 0.15 mm/rev, an increase of about 4456 % (11 against 500 holes) was observed. It is important mentioning that at the higher cutting speed, the adopted end of tool life criterion based on the maximum flak wear was not reached.

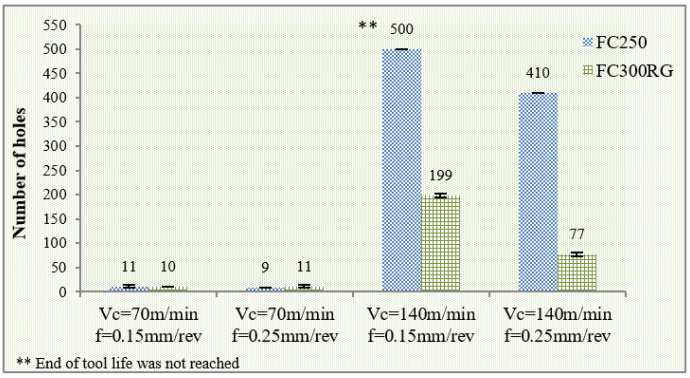

Figure 6. Results of the tool life tests of the two work materials investigated (end of tool life criterion: $VB_{Bmáx}$ = 0.4 mm or 500 holes)

In order to find reasons for this adverse behavior, i.e., the number of holes increases substantially with increasing cutting speed, it is proposed that a comparison of the wear mechanisms found in the tools used in this work. In general, the wear mechanisms found on the drills used to machine the gray irons follow the pattern shown in the adapted diagram of Fig. 7. From this analysis, it appears that with increasing speed, the adhesive wear mechanism - also called attrition (Trent, 200) - has been reduced and replaced by diffusion that gradually takes place and predominates. Thus, it is suggested that the type of tool used in the drilling tests performs better when subjected to the action of the latter mechanism mentioned and a worse performance under the action of adhesion (attrition) mechanism.

By analyzing the morphology of the wear suffered by the drills used in the machining of the materials investigated under the high cutting speed condition (140 m/min) (at both feed rates 0.15 mm/rev and 0.25 mm/rev), it appears that the wear on tools are very shallow, only a few and isolated islands of the worn region the substrate is reached (as can be seen in Fig. 7). This means that the tool life, according to the adopted end of tool life criteria, is strongly governed by the wear resistance of the coating (TiAlN). It is also observed that the predominant wear mechanism is diffusion - the wear scar has a polished aspect (smooth). By comparing the machining of the two materials under the lower cutting speed of 70 m/min when the tools are worn mainly by adhesion (or attrition) - because the wear morphology is rough - two interesting aspects are verified.

Firstly, the adhesive wear rate that prevails in the lower cutting speed was higher than the rate of diffusion wear, predominantly in machining at higher cutting speeds. Secondly, the FC300RG showed lower machinability at high cutting speed compared to the FC250, this because the prevailing wear mechanism, diffusion is strongly dependent on the temperature and this material having higher mechanical strength and hardness, will require greater energy in

machining, developing a higher temperature. At the lowest shear rate (lower cutting speed), the prevailing wear mechanism, adhesion, which depends less on the temperature and more on the ability of the work material to adhere onto the surface of the tool and on the irregular form that the adhered material flows when shearing, the results demonstrated that the higher mechanical strength of the FC300$_{RG}$ gray cast iron is not significant in this process.

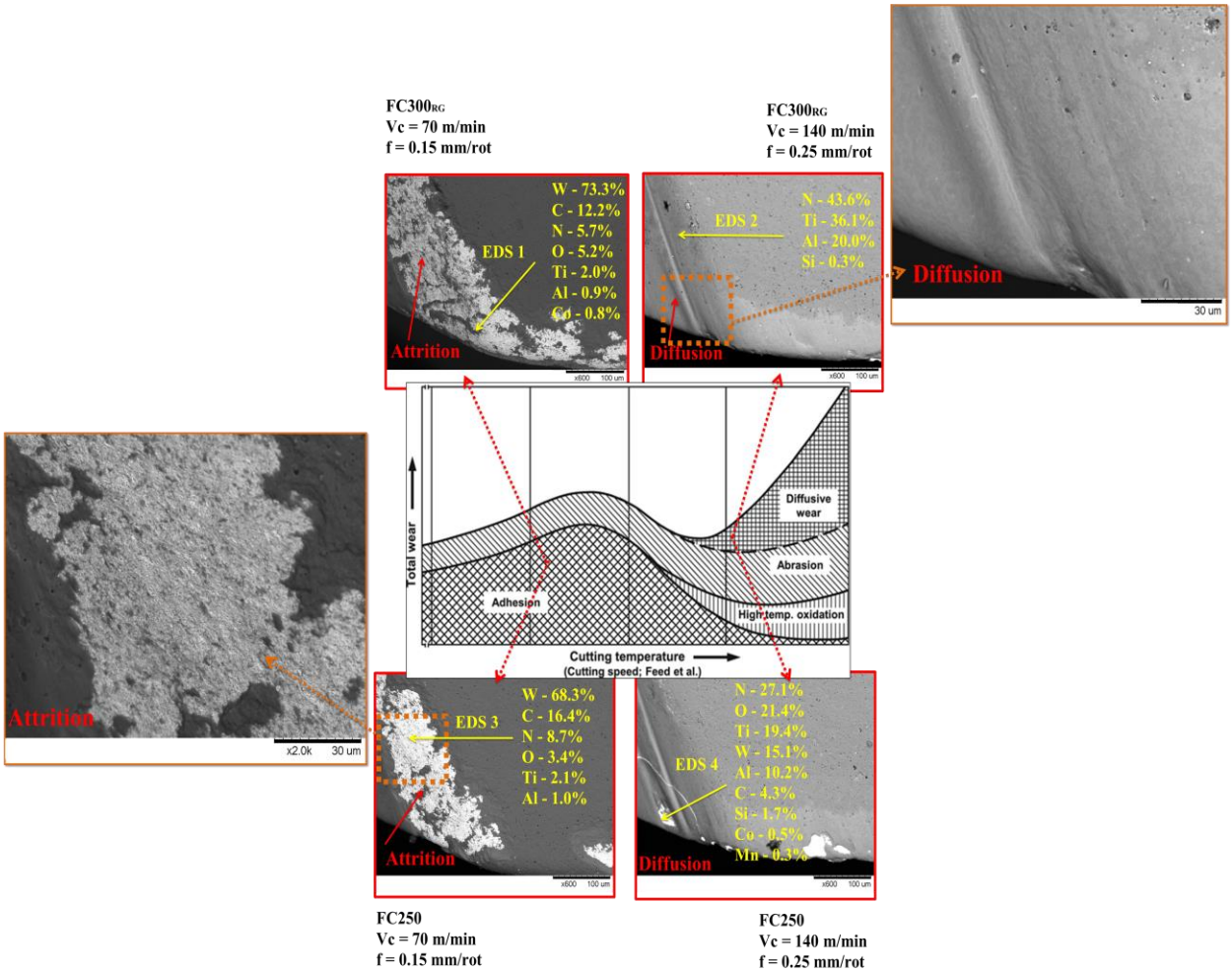

Figure 7. Wear mechanism as a function of the cutting speed (Adapted König and Klocke, 2008)

3.3 Significance analysis of the results of tool life

Ignoring the effect of the interaction between the feed rate and the work material (for other variables can become significant) a significance analysis of the tool life results was performed for comparison of the two materials, considering the four cutting conditions tested. Table 5 shows this analysis, with a reliability of 95% and 5% significance level (p), using Statistica 7.0 software.

Table 5. Significance analysis of the tool life results of the two work materials tested: FC250 e FC300$_{RG}$

Fator	Effects (holes)	p-value
Mean	161.250	0.003883
Cutting speed (Vc) [m/min]	297.500	0.004559
Feed rate (f) [mm/rev]	-45.000	0.155218
Work material	-165.000	0.014596
Interaction between Vc x f	-45.000	0.155218
Interaction between Vc x work material	-165.000	0.014596

In the comparison between the FC250 and FC300RG, a significant difference between these materials is observed. Because the p-values are lower than 0.05, the type of work material, the cutting speed and the interaction between them have significant effects on the results. In the column of the effects of Tab. 5, it is clear that, with increasing cutting speed, there was an increase in the number of holes machined, an average of 298. However, the change of the work material from FC250 to FC300RG, a reduction in the number of holes is observed, an average of 165 holes. Finally, the interaction between Vc and type of gray cast iron has also reduced the number of drilled holes, average of 165 holes, by moving from level (-1) to level (+1). This result demonstrates the good machinability of the FC250 because of its lower tensile strength and hardness, in that both properties are configured as a reflection of the greater spacing between the lamellae of Fe_3C, lower microhardness of pearlite and less eutectic cells per cm^2, among others, in comparison to FC300RG.

3.4 Results of the thrust force (Fz) and torque (Mz)

Figures 8 and 9 illustrate, respectively, the behavior of the thrust force Fz and torque Mz when varying the cutting speed and feed rate, respectively.

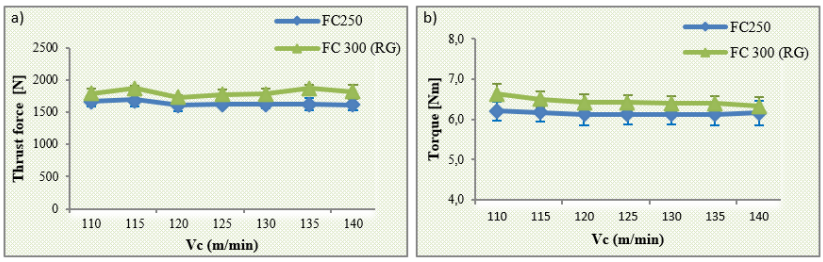

Figure 8. Behavior of a) Thrust force (Fz); b) Torque (Mz) against the cutting speed

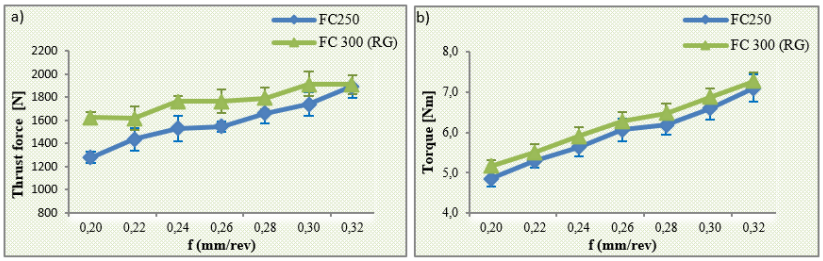

Figure 9. Behavior of a) Thrust force (Fz); b) Torque (Mz) against the feed rate.

The results of the plots in Fig. 8 show that both the thrust force and torque remained approximately constant, meaning that the cutting speed did not affect these machining parameters significantly, in the tested range. The average results Fz and Mz were slightly higher for the FC300RG compared to FC250. In the analysis of Fig. 9, it is possible to observe a slight trend of increase in the Fz component as the feed rate is increased. In somewhat more pronounced, with increasing feed rate the torque also increases. According to Barbosa *et al*. (2009), the increment of this variable directly increases the areas of primary and secondary shear, causing the increase of Fz and Mz (BARBOSA, 2009).
Also, the higher the feed rate, the greater is the plastic deformation and work hardening of the chip by the drill in bottom of the hole. Thus, there is a greater resistance to penetration of the drill due to the combined effect of crushing the material in the chisel edge and cutting of the material in the two main cutting edges (SOUZA et. al, 2014). As with the previously discussed condition (Fig. 8), the two gray cast irons showed similar values of thrust force and torque. Again, the mean values of Fz and Mz were slightly higher for the FC300RG, indicating the possible interference of the refined graphite and larger number of eutectic cells on the results thrust force and torque.

3.5 Results of the thrust force (Fz) and torque (Mz)

The plots of Fig. 10 illustrate the variation of surface roughness parameter *Ra* against to the variation of cutting speed and feed rate. It can be seen that the roughness parameter *Ra* showed no clear trend with increasing cutting speed and feed rate, in addition to being quite similar for the two materials. According to Machado *et al*. (2015), the increase in the feed rate should increase the height of the peaks and the depth of the valleys impacting the roughness of the surface (MACHADO *et. al*, 2015). However, this conventional effect was not observed, possibly due to the favorable shape of the edge on the tips of the drills. As general comments, the *Ra* values, when varying the cutting speed, was slightly higher for the FC300RG gray cast iron as compared to the FC250 (Fig. 10a). On the other hand, when varying the feed rate, in general, Ra values were lower for the FC300RG. This fact can be justified, according to Machado *et al*.

(2015), by the better mechanical properties of the gray cast iron with refined graphite, so that the greater the hardness of the material the better tends to be the surface roughness .

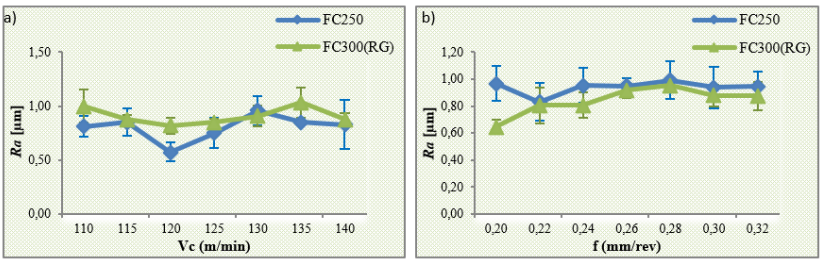

Figure 10. Variation of surface roughness, Ra a) against Vc; b) against f.

Figures 11 and 12 show the results of roundness and cylindricity when varying the cutting speed and feed rate, respectively.

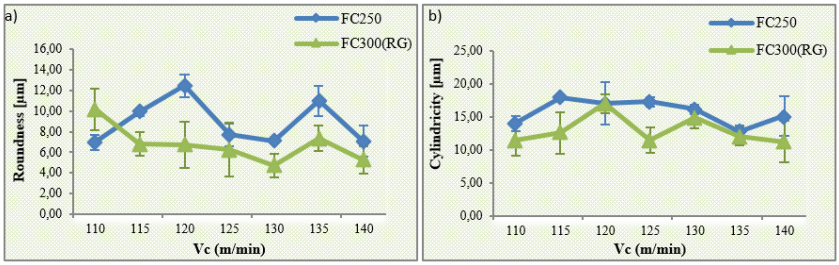

Figure 11. Form deviation against cutting speed: a) roundness; b) cylindricity

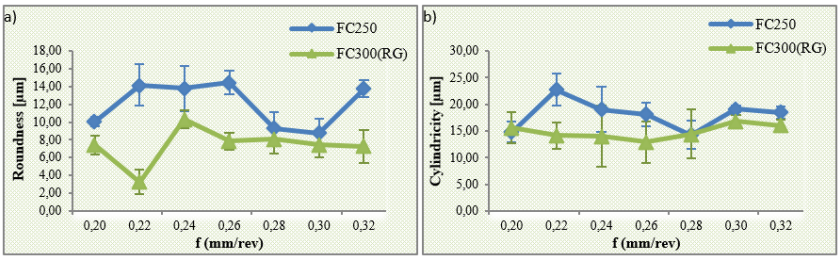

Figure 12. Form deviation against feed rate: a) roundness; b) cylindricity

By analyzing the plots of Figs. 11 and 12 it can be seen that the form deviations studied did not show a defined trend when varying the cutting speed and the feed rate. It can be concluded that in some cases due to the standard deviation bars statistical differences become irrelevant. However, in general, it is clear that among all the tested conditions in a total of 28 points (14 points varying the cutting speed and 14 points varying the feed rate), more than half of the values encountered (roundness and cylindricity) were lower for the FC300$_{RG}$ compared to FC250. These results may have shown the influence of the refined graphite of the FC300$_{RG}$ in the hole qualities. The chip formation in the gray iron is related to fracture in front of the cutting region where the more refined is the graphite smaller will be the lamellae of the chips formed by the fracture, which may result in a better quality in the form of drilled holes compared the gray cast iron with larger veins and thicker graphite.

4. CONCLUSIONS

This work provides a comparison on the use of FC-300 with the addition of Mo and refined graphite in the production of cylinder heads for diesel engines. From the point of view of the technological aspects of machining, FC300$_{(RG)}$'s behavior in the tests carried out in this research showed, without doubt, that the application of this material is promising. During some trials, such as those of thrust force and torque, only slightly higher values for the gray iron with refined graphite compared to gray iron FC250 was observed. Furthermore, with regard to the quality of the holes, the FC300$_{RG}$ also showed satisfactory results. Another important aspect of this work refers to the performance of the drills when subjected to machining at lower cutting speed (70 m/min), which shows a premature wear behavior for the materials studied. In this condition the tools worn out predominantly by adhesion (attrition). However, with increasing cutting speed up to 140 m/min, the wear by attrition was losing space for the phenomenon of diffusion, which may be connected to the better performance of the drills used in tool life tests for the condition of higher cutting speed, regardless the feed rate used.

However, in order to better quantify the machinability of this material, it is suggested new studies (e.g., evaluating the machinability of these materials by applying other machining processes such as milling, turning, reaming and tapping) that have different methods from those used in this research. It is also suggested to use more aggressive end of tool life life criteria, such as collapsing of the drill.

5. ACKNOWLEDGEMENTS

The authors would like to thank CAPES, CNPq and FAPEMIG for financial support, the Tupy S.A for supplying the work materials, and ISCAR Brazil Ltda. for providing the tools.

6. REFERENCES

ABNT NBR ISO 4288 - Especificações geométricas de produto (GPS) - Rugosidade: Método do perfil - Regras e procedimentos para avaliação de rugosidade, 2008.

ASM Handbook Committee - Properties and selection - Nonferrous alloys and special-purpose materials. 10 ed. USA: ASM International, 1990b. Vol. 2. P. 3470.

ASM Handbook Committee- Properties and selection – Irons, Steels, and High-Performance Alloys. 10 ed. USA: ASM International, 1990a. Vol. 01. p. 1063.

ASM Handbook Committee. Machining. 9 ed. USA: ASM International, 1989. Vol. 16. p. 1089.

ASTM A247, Standard Test Method for Evaluating the Microstructure of Graphite in Iron Castings, 2010.

Azterlan Research Aliance. Superfine Graphite Gray Cast Iron: High Ultimate Tensile Strength Combined with Low Hardness. 2013. Available on: <http://www.azterlan.es/es/index.aspx>. Accessed: 21 september. 2014.

Barbosa. P. A; Rabelo, G. B.; Guesser, W. L.; Costa; E. S.; Machado, A. R. Force and Torque when Drilling Ductile Cast Iron and Compacted Graphite iron. In: V Brazilian Congress of Mechanical Engineering (COBEF). 2009. Belo Horizonte – MG.

Bates, C. E. Study examines influences on machinability of iron castings. Modern Castings, pp. 36-39, out. 1996.

Dawson, S. Compacted graphite iron – A material solution for modern diesel engine cylinder blocks and heads. China Foundry, v. 6, pp. 241-246, ago. 2009.

Guesser, W. L. Propriedades Mecânicas dos Ferros Fundidos. 1. ed. São Paulo: Blücher, 2009. p. 336.

König, W.; Klocke, F. Fertigungsverfahren: Drehen, Frasen und Bohren. Berlim: Heidelberg, 2008. p. 562.

Machado, Á. R.; Abrão, A. M.; Coelho, R. T.; da Silva, M. B. Teoria da Usinagem dos Materiais. 3. ed. São Paulo – SP: Edgard Blücher, 2015. p. 407.

Marquard, R.; Helfried, S.; Mcdonald, M. New materials create new possibilities. Engine Technology International, vol. 2, pp. 58-60, 1998.

Marwanga, R. O. , Voigt, R. C. , Cohen, P. H. Influence of Graphite Morphology and Matrix Structure on Chip Formation During Machining of Continuously Cast Ductile Irons. AFS Transactions: American Foundrysmen Society. Detroit . pp. 651-661, 2000.

Marwanga, R. O. ; VoigT, R. C. ; Cohen, P. H. Influence of Graphite Morphology and Matrix Structure on Chip Formation During Machining of Gray Irons. AFS Transactions: American Foundrysmen Society. Detroit . pp. 595-607, 1999.

Röhrig, K. Niedriglegierte Graphitische Gusseisenwerkstoffe – Eigenschaften und Anwendung. Konstruiren + Giessen, v.6, n. 3, pp. 4 – 21, 1981.

Souza, A. J.; Mattes, F. B.; Mognaga, G. F. Analysis of Cutting Forces Generated in Drilling of Din GGG50 with Carbide Drills for Changed Micro-Geometries. In VIII National Congress of Mechanical Engineering (CONEM), 2014. Uberlândia – MG.

Trent, M. C., Wright, P. K., Metal Cutting Principles. 4th edition. Butterworth – Heinemann, USA, 2000.

TUPY, S.A. Perfis de Fundição Contínua. 2014. p. 34. Technical Reports.

Voort, G. F. V.; Roosz, A. Measurement of the Interlamellar Spacing of Pearlite. Metallography, v. 17, pp. 1-17, 1984.

7. RESPONSIBILITY NOTICE

The authors are the only responsible for the printed material included in this paper.